Available online at www.sciencedirect.com
ScienceDirect
Trans. Nonferrous Met. Soc. China 30(2020) 2067−2078
Transactions of Nonferrous Metals Society of China
www.tnmsc.cn

Effect of Zn/Mg ratio on cathodic protection of carbon steel using Al−Zn−Mg sacrificial anodes

Mosaad SADAWY[1], Saad SAAD[1], Randa ABDEL-KARIM[2]

1. Department of Mining and Petroleum Engineering, Faculty of Engineering, Al-Azhar University, Nasr City, Cairo 11371, Egypt;
2. Department of Metallurgy, Faculty of Engineering, Cairo University, Giza 12613, Egypt

Received 22 August 2019; accepted 29 May 2020

Abstract: Al−Zn−Mg alloys with different Zn/Mg mass ratios were evaluated as sacrificial anodes for cathodic protection of carbon steel in 3.5 wt.% NaCl solution. The anodes were fabricated from pure Al, Zn and Mg metals using casting technique. Optical microscopy, SEM−EDS, XRD and electrochemical techniques were used. The results indicated that with decreasing Zn/Mg mass ratio, the grain size of α(Al) and the particle size of the precipitates decreased while the volume fraction of the precipitates increased. The anode with Zn/Mg mass ratio >4.0 exhibited the lowest corrosion rate, while the anode with Zn/Mg mass ratio <0.62 gave the highest corrosion rate and provided the highest cathodic protection efficiency for carbon steel (AISI 1018). Furthermore, the results showed that the anode with Zn/Mg mass ratio <0.62 exhibited a porous corrosion product compared to the other anodes.

Key words: cathodic protection; Al−Zn−Mg sacrificial anode; current capacity; passive film; precipitate; grain size

1 Introduction

Cathodic protection is the most important technique used to protect steel structures from corrosion attack in different environments [1,2]. Nowadays, cathodic protection using the sacrificial anodes in the marine environments is widely applied [3,4]. Al anodes attract attention of many companies due to their high theoretical cell voltage and energy density (8076 W·h/kg [5−8]. However, the main problem is that Al anodes passivate spontaneously when they are in contact with air or aqueous electrolytes [9]. Owing to this film, the corrosion potential (φ_{corr}) of the anode is moved to a more positive value, and the dissolution activity of anodes is decreased [10].

The success of aluminum as a sacrificial anode depends greatly on some alloying elements such as Hg, Si, Ti, Sn, Pb, Ga and In [11−15]. These elements prevent the formation of continuous passive film on the surface of aluminum, consequently, permitting continuous galvanic reaction [12]. Although these elements increase the activation of aluminum as a sacrificial anode, finding a replacement way for them is very important, because Hg is very toxic, Ga is very expensive and In is not suitable for all environments [16].

Many investigators pointed that Al−Zn−Mg alloys are promising alloys for cathodic protection owing to its high current capacity, low electrode potential and the absence of Hg and In [17]. Al−Zn−Mg alloys are a multi-component system of Al, Zn and Mg, which possess high hydrogen over potential [18]. Therefore, the elemental mass ratio of Al−Zn−Mg system is a key factor influencing shape, size and distribution of precipitates as well as, segregation along the grain boundary which in turn play a complex role in the matrix. On one side

Corresponding author: Mosaad SADAWY; Tel: +20-1113302663; E-mail: mosaadsadawy@yahoo.com
DOI: 10.1016/S1003-6326(20)65361-4

they increase the strength of the alloy; on the other side they increase its corrosion rate [19]. It has been reported that the main precipitate in Al−Zn−Mg system is $MgZn_2$ which works as an anode while α(Al)-matrix works as a cathode. FAYED et al [18] have shown that such intermetallic particles in Al–Zn–Mg system are dissolved faster than the Al-rich matrix and uniform corrosion could be obtained by controlling the uniform distribution of the precipitate. OROZCO et al [20] investigated the effect of magnesium on the electrochemical behavior of Al−Zn−Mg. The content of magnesium was ranged from 5.5 at.% to 8.5 at.%. It was found that increasing magnesium leads to an enhancement in electrochemical behavior of aluminum. Therefore, it is very meaningful to investigate the influence of Zn/Mg mass ratio on the microstructure and corrosion behavior of as-cast Al−Zn−Mg sacrificial anodes.

In the present investigation, a series of Al−Zn−Mg ingots with different Zn/Mg mass ratios were fabricated. The microstructure and corrosion properties were analyzed and discussed. Additionally, the cathodic protection of steel (AISI 1018) using theses anodes was investigated and discussed.

2 Experimental

2.1 Materials

The Al−Zn−Mg alloys used in this investigation were produced using casting technique. Pure Al was melted in muffle furnace. After melting, a certain amount of Zn was added gradually and stirred using graphite rod for 3 min. After that a certain amount of pure Mg was also added gradually and stirred also for 3 min. The slag was removed before pouring. Finally, the molten alloys were cast in steel mold with dimensions of 200 mm × 50 mm × 20 mm. After casting, the samples were chemically analyzed using XRF (Table 1) and cut into dimensions of 30 mm × 10 mm × 10 mm for the cathodic protection tests.

The anode samples were prepared for microstructure by grinding with 360−1500 grit SiC papers and polished using cloth and diamond paste with 6, 3 and 1 μm, respectively. After that the samples were cleaned using water and acetone and dried in air. Keller solution was used for etching all samples.

Table 1 Chemical composition of Al−Zn−Mg anodes (wt.%)

Anode No.	Fe	Si	Zn	Cu	Mn	Mg	Al	Zn/Mg mass ratio
1	0.226	0.108	3.92	0.012	0.005	0.960	Bal.	4.08
2	0.190	0.097	5.25	0.009	0.009	1.860	Bal.	2.82
3	0.225	0.110	3.25	0.018	0.018	3.120	Bal.	1.04
4	0.136	0.067	1.93	0.002	0.016	3.21	Bal.	0.60

Carbon steel sheets (AISI 1018) with chemical composition presented in Table 2 were used as a cathode in the cathodic protection tests. Samples with dimensions of 50 mm × 20 mm × 5 mm were prepared.

Table 2 Chemical composition of carbon steel alloy (AISI 1018) (wt.%)

C	Si	P	S	Mn	Fe
0.14	0.26	0.051	0.03	1.02	Bal.

2.2 Electrochemical measurements

2.2.1 Potentiodynamic polarization

The Potentiodynamic polarization test was performed using Potentiostat/Galvanostat (EG&G model 273). M 352 corrosion software was used for extracting corrosion parameters. All samples were polished to 1200 grit and cleaned with distilled water and acetone. A three-electrode system consisted of working electrode (Al−Zn−Mg alloys) with 1.0 cm^2 of surface area, counter electrode (Pt sheet) and reference electrode (Ag/AgCl) was used. The polarization test was carried out by changing the electrode potential, including compensation for the ohmic drop potential of the solution at a scan rate of 0.5 mV/s (after OCP was stable for ~30 min) and a potential range of ±250 mV (φ_{corr}). These values were selected to simultaneously shorten the measurement time and minimize the capacitive current. A similar scan rate was used by MA et al [21] and LI et al [7]. The PAR Calc Tafel Analysis routine statistically fits the experimental data to the Stern−Geary model for a corroding system. The routine automatically selects the data that lie within the Tafel region and calculates the corrosion current and the corrosion rate.

2.2.2 Cyclic polarization

Cyclic polarization test was performed from −100 mV (φ_{corr}) towards the anodic direction at a scan rate of 1 mV/s to simultaneously shorten the

measurement time and minimize the capacitive current. This value is similar also to that of MA et al [21] and LI et al [7]. The potential scan was reversed when the current density reached 10 mA/cm^2.

2.2.3 Cathodic protection tests

The steel samples and Al−Mg−Zn sacrificial anodes were weighed and coupled together using Cu wire. After that the samples were immersed into the electrolyte. The reference electrode (Ag/AgCl) and the steel samples with Al−Mg−Zn sacrificial anodes were connected together with a digital multimeter (DT9200A) for measuring the potential. After dipping into the electrolyte for 90 d, the specimens were removed, cleaned using 1 mol/L HNO_3 solution for 3 min and dried. Then the specimens were reweighed. The corrosion rates of steel and Al−Mg−Zn sacrificial anodes were calculated using Eq. (1) [10,18]:

$$r=\frac{K\Delta W}{ADt} \tag{1}$$

where r is the corrosion rate (mm/a), K is a constant (8.76×10^4), ΔW is the mass loss (mg), A is the surface area (cm^2), D is the density (g/cm^3) and t is the time (h).

All corrosion and cathodic protection tests were performed in a 3.5 wt.% NaCl solution which was prepared with analytical grade chemicals. The cathodic protection efficiency of steel connected with different Al−Zn−Mg sacrificial anodes was calculated according to Eq. (2):

$$\eta=\left(1-\frac{r_{\text{corr}}}{r_{\text{corr}}^0}\right)\times100\% \tag{2}$$

where η represents the cathodic protection efficiency (%); r_{corr} and r_{corr}^0 are the corrosion rates of steel (mm/a) with and without Al−Mg−Zn sacrificial anodes, respectively.

Three separate experiments were performed for each run to ensure the reproducibility of results. The standard deviation value in each condition was calculated to assess the statistical error.

2.3 Surface analysis

The microstructure and surface morphologies of anodes and steel samples were performed using scanning electron microscopy (SEM), energy-dispersive X-ray spectroscopy (EDS) model JEOL JSM−6330F, Olympus optical microscope and X-ray diffraction analysis (Philips Machine).

3 Results and discussion

3.1 Microstructures

The microstructures of the investigated ingots with different Zn/Mg mass ratios are shown in Fig. 1. It can be seen that all alloys indicate a

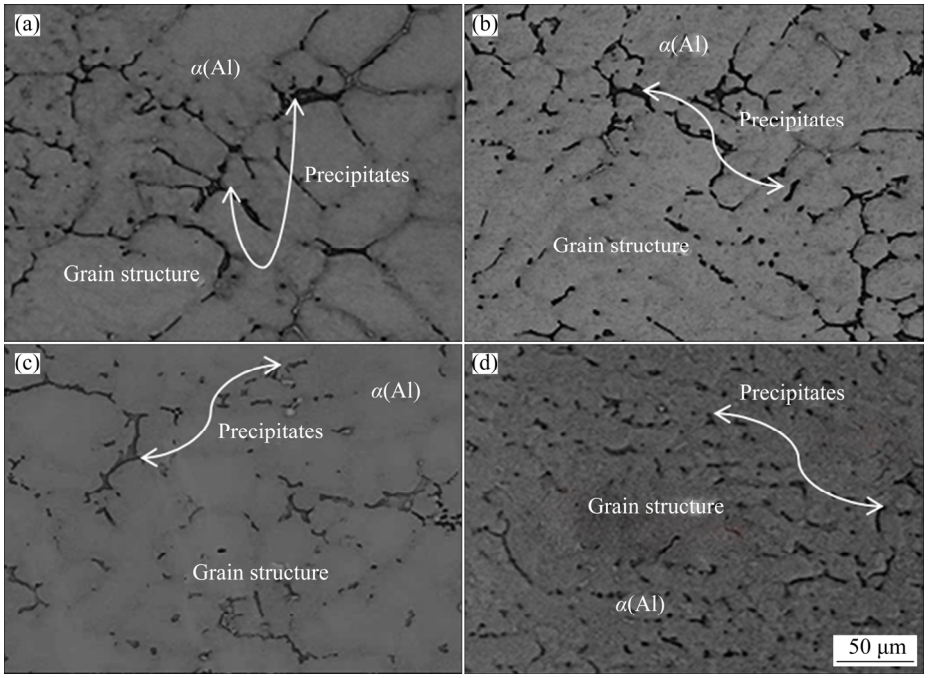

Fig. 1 SEM images of investigated anodes with different Zn/Mg mass ratios: (a) Anode 1; (b) Anode 2; (c) Anode 3; (d) Anode 4

dendritic microstructure, while the precipitates exist between the arms of the dendrite. The average grain size of the as-cast alloys grows with increasing Zn/Mg mass ratio. The backscatter SEM images as shown in Fig. 2 reveal that the precipitates locate along the grain boundaries forming a network-shaped phases for all ingots. However, these precipitates become larger with increasing Zn/Mg mass ratio. The behavior is due to diffusing large amount of Zn and Mg from the rich zone in the center of α(Al) grain to the neighboring regions. Also, it can be noted that no discernable fine particles are observed in the α(Al) grains. A similar microstructure was commonly reported elsewhere [22−24]. The volume fraction of the precipitates estimated using ImageJ is shown in Fig. 3. It is obvious that the volume fraction of the precipitates increased with decreasing Zn/Mg mass ratio. The behavior may be attributed to the nucleation activation energy of the precipitates which is controlled by the Zn/Mg mass ratio [25]. The EDS analysis (Fig. 4) displays the composition of marked precipitates. The results illustrate that these precipitates are composed of Al, Zn and Mg with different Al, Zn and Mg contents presented in Table 3.

To validate the results obtained from the SEM−EDS, a phase analysis using XRD was performed. Figure 5 shows that the investigated ingots contain α(Al) solid solution with $MgZn_2$ and $Mg_{32}(Al,Zn)_{49}$ precipitates.

3.2 Corrosion behavior

3.2.1 Potentiodynamic polarization

The effect of Zn/Mg mass ratio on the polarization behavior of the as-cast Al−Zn−Mg alloys is shown in Fig. 6. The curves show that the cathodic and anodic current densities increase with the decrease of Zn/Mg mass ratio. The cathodic reaction according to Eq. (3) is the oxygen reduction reaction (ORR) [10]:

$$O_2+2H_2O+4e\rightarrow 4OH^- \quad (3)$$

Similarly, QUEVEDO et al [26] found that the cathodic behavior on the surface of Al−Zn−Mg alloy in synthetic sea water revealed a reduction process dominated by a single wave for reduction of oxygen in a potential range of −1000 to −1200 mV (vs SCE). Further, their results indicated that a slightly production of hydrogen peroxide was obtained. This behavior means that the ORR is a mass-transfer-controlled regime proceeding through a pathway reduction mechanism involving a four-electron process.

The elementary reaction steps on the surfaces of Al−Zn−Mg alloys are in the following reaction

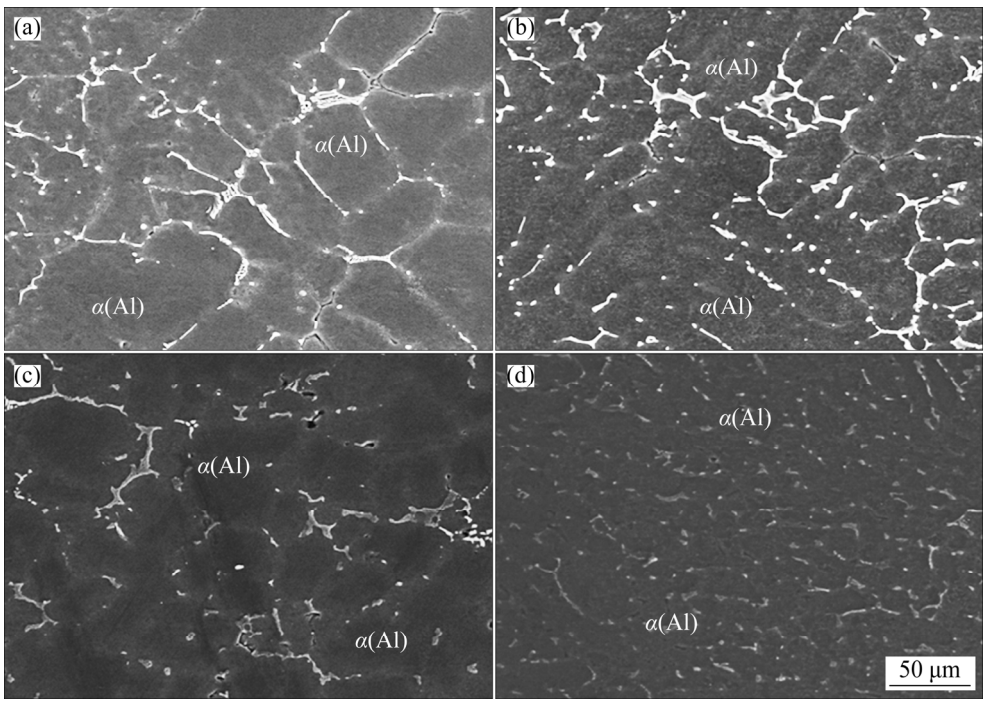

Fig. 2 Backscatter SEM images of anodes with different Zn/Mg mass ratios: (a) Anode 1; (b) Anode 2; (c) Anode 3; (d) Anode 4

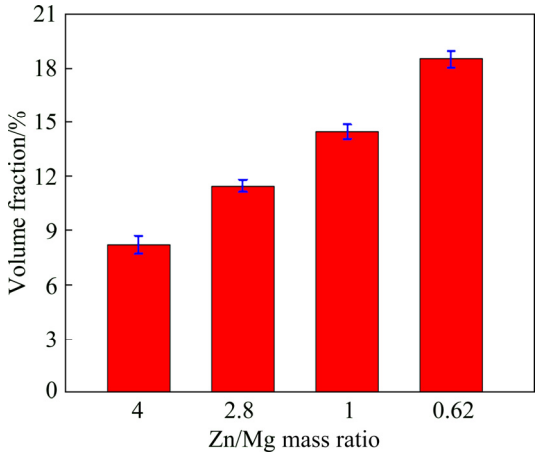

Fig. 3 Effect of Zn/Mg mass ratio on volume fraction of precipitates for Al−Zn−Mg sacrificial anodes

paths [27]:

$$O_2(g)+2H_2O(l)+4e+*\rightarrow OOH*+OH^-+H_2O(l)+3e \quad (4)$$

$$OOH*+OH^-+H_2O(l)+3e\rightarrow O*+2OH^-+2H_2O(l)+2e \quad (5)$$

$$O*+2OH^-+H_2O(l)+2e\rightarrow OH*+3OH^-+e \quad (6)$$

$$OH*+3OH^-+e\rightarrow 4OH^- \quad (7)$$

The increase of cathodic current densities with decreasing Zn/Mg mass ratio is attributed to increasing the defects in the passive film. This leads to increasing the density of oxygen vacancies and hence the oxygen reduction rate is increased.

The anodic reactions occurring on the surface are the dissolutions of Mg, Zn and Al according to Eqs. (8)−(10):

$$Mg\rightarrow Mg^{2+}+2e \quad (8)$$

$$Zn\rightarrow Zn^{2+}+2e \quad (9)$$

$$Al\rightarrow Al^{3+}+3e \quad (10)$$

The electrochemical parameters were extracted from Fig. 6 and presented in Table 4. It can be seen from Table 4 that the J_{corr} for Alloy 4 is the highest, while the φ_{corr} is the lowest. This behavior is attributed to increasing the volume fraction of precipitates during the solidification and forming micro galvanic cell with α(Al) matrix. On the other hand, Alloy 1 exhibits the lowest J_{corr} value and the highest φ_{corr} value. The behavior is due to coarsening the grains. According to many authors [28], coarsening the grains leads to decreasing the volume fraction of the precipitate and hence, increases the corrosion resistance. On the contrary,

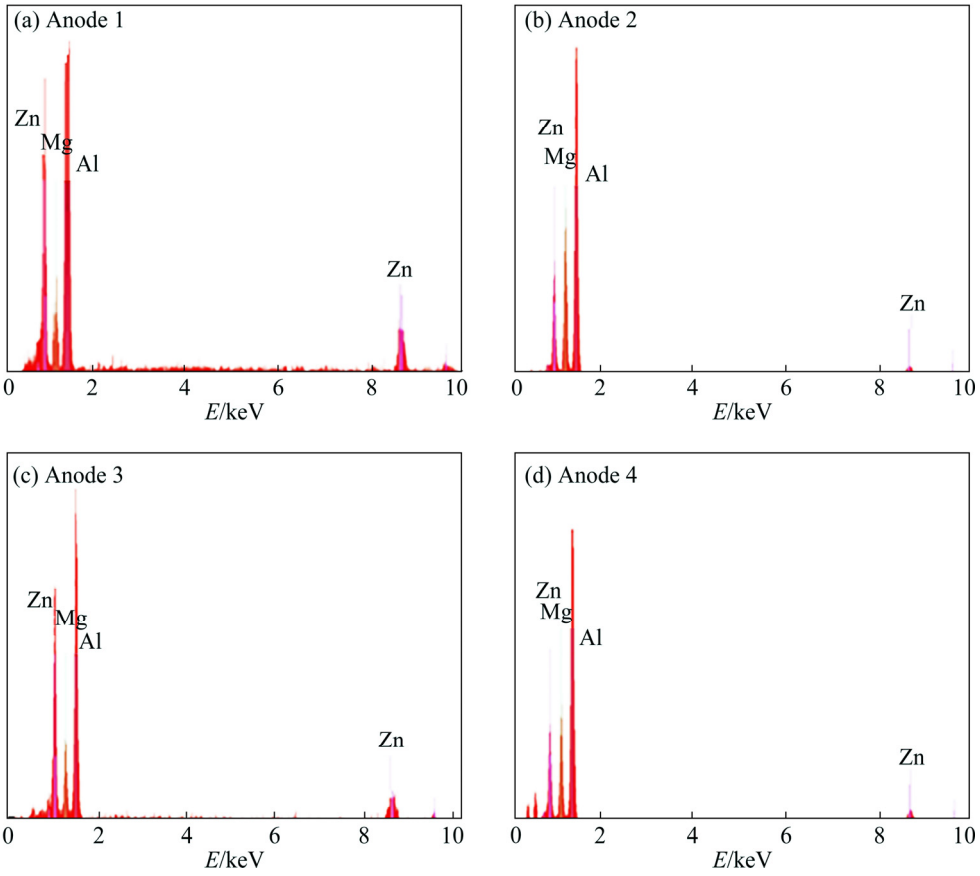

Fig. 4 EDS results of investigated ingots

Table 3 Chemical composition of precipitates determined by EDS (wt.%)

Anode No.	Zn	Mg	Al
1	45.04	9.22	45.74
2	33.54	14.05	52.41
3	21.94	18.85	59.21
4	17.90	22.50	59.60

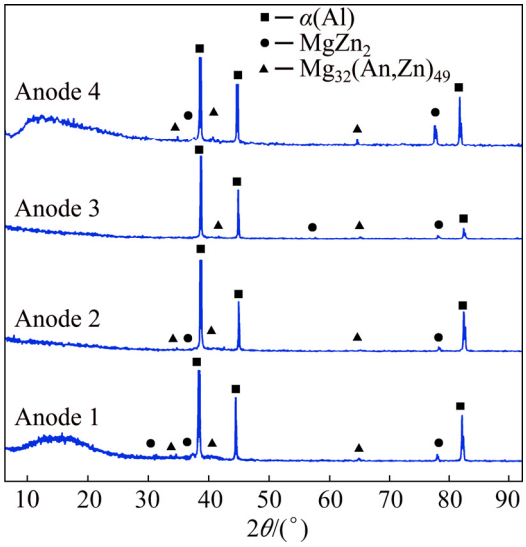

Fig. 5 XRD patterns of investigated ingots

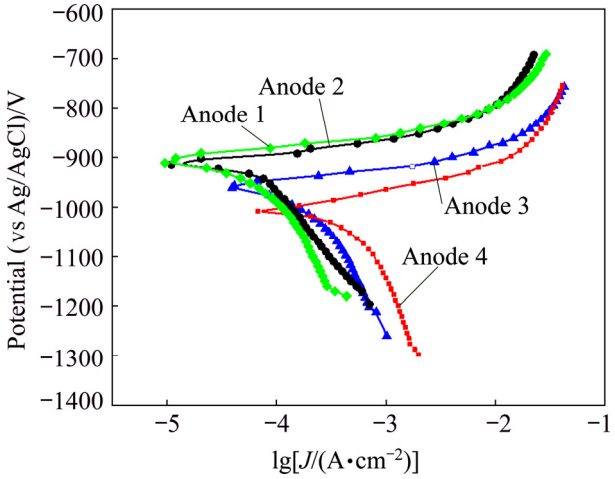

Fig. 6 Potentiodynamic polarization curves of Al−Zn−Mg anodes with different Zn/Mg mass ratios in 3.5 wt.% NaCl solution

the corrosion rate increases due to increasing densities of grain boundaries, which offer more sites for initiation of corrosion, especially if the precipitates are segregated along the grain boundaries [28]. Table 4 also shows that the anodic slopes (β_a) have closed values ranging from 90 to 73 mV/decade. This means that all investigated ingots have the same anodic dissolution mechanism.

Table 4 Corrosion parameters of Al−Zn−Mg with different Zn/Mg mass ratios in 3.5 wt.% NaCl solution

Anode No.	φ_{corr}/ mV	J_{corr}/ (A·cm^{-2})	β_c/ (mV·dec^{-1})	β_a/ (mV·dec^{-1})
1	−925±3	(8.71±0.3)×10^{-5}	130±4	90±5
2	−930±4	(1.26±0.2)×10^{-4}	141±2	83±7
3	−985±5	(5.16±0.4)×10^{-4}	165±3	77±4
4	−1050±3	(8.42±0.5)×10^{-4}	175±3	73±5

The morphologies after potentiodynamic polarization are shown in Fig. 7. The morphologies show that Alloys 1 and 2 (Figs. 7(a, b)) exhibited resistance to corrosion by forming compact corrosion products on the surface. However, they were attacked with pitting and intergranular corrosion at grain boundaries due to depletion of the precipitates. Moreover, Figs. 7(c, d) show that Alloys 3 and 4 heavily corroded with porous corrosion products.

3.2.2 Cyclic polarization

The effect of Zn/Mg mass ratio on the passive stability and susceptibility to localized attack was investigated by cyclic polarization, as shown in Fig. 8. All curves were plotted individually to avoid complexity. The curves show active, passive and trans-passive regions. However, the range of passivity grows gradually with increasing Zn/Mg mass ratio. It is known that the intermetallic precipitates weaken the passive film by breaking its continuity [18]. Coarsening the grains by increasing the Zn/Mg mass ratio, causes a reducing in the densities of grain boundary and volume fraction of these precipitate inside the matrix. This provides more protective passive zones on the surface. Further, it is interestingly to note that small areas of the hysteresis loops are obtained for all investigated ingots, suggesting a decrease of pitting during the reverse scan due to the formation of black layers. Table 5 presents the cyclic polarization parameters obtained from Fig. 8. It is clear that more positive pitting potential is obtained by increasing Zn/Mg mass ratio. This signifies harder breakdown of the passive film. Additionally, Table 5 indicates that the protection potential of Al−Zn−Mg ingots is lower than the φ_{corr}. This means that all investigated ingots have not the ability to re-passivate.

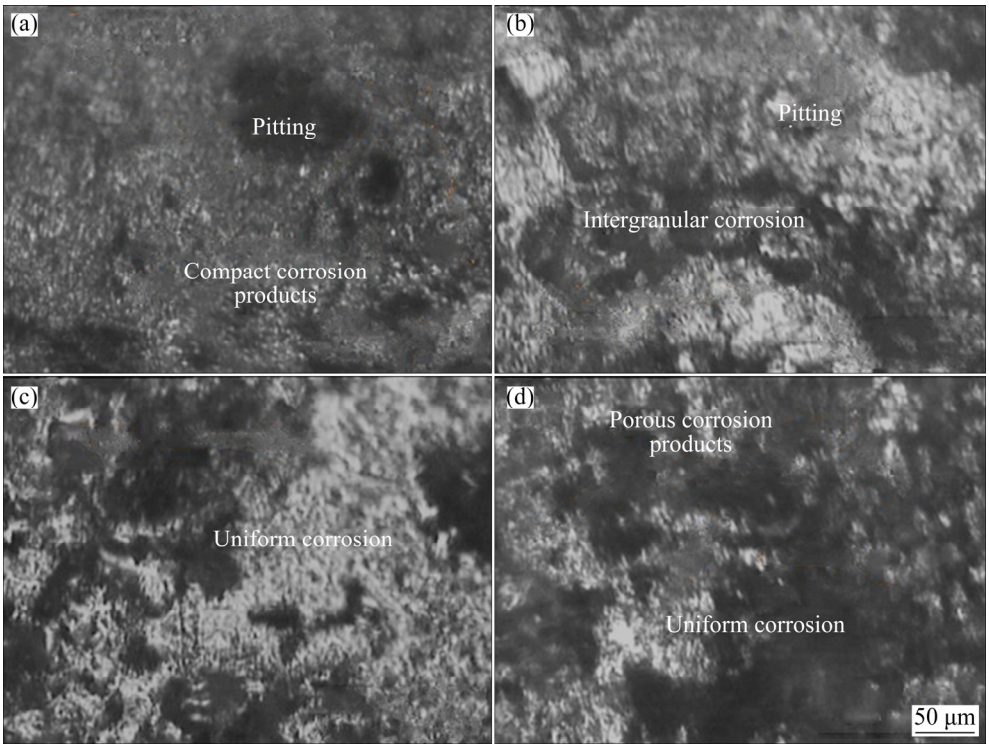

Fig. 7 Optical micrographs of surface morphologies of anodes after potentiodynamic polarization tests: (a) Anode 1; (b) Anode 2; (c) Anode 3; (d) Anode 4

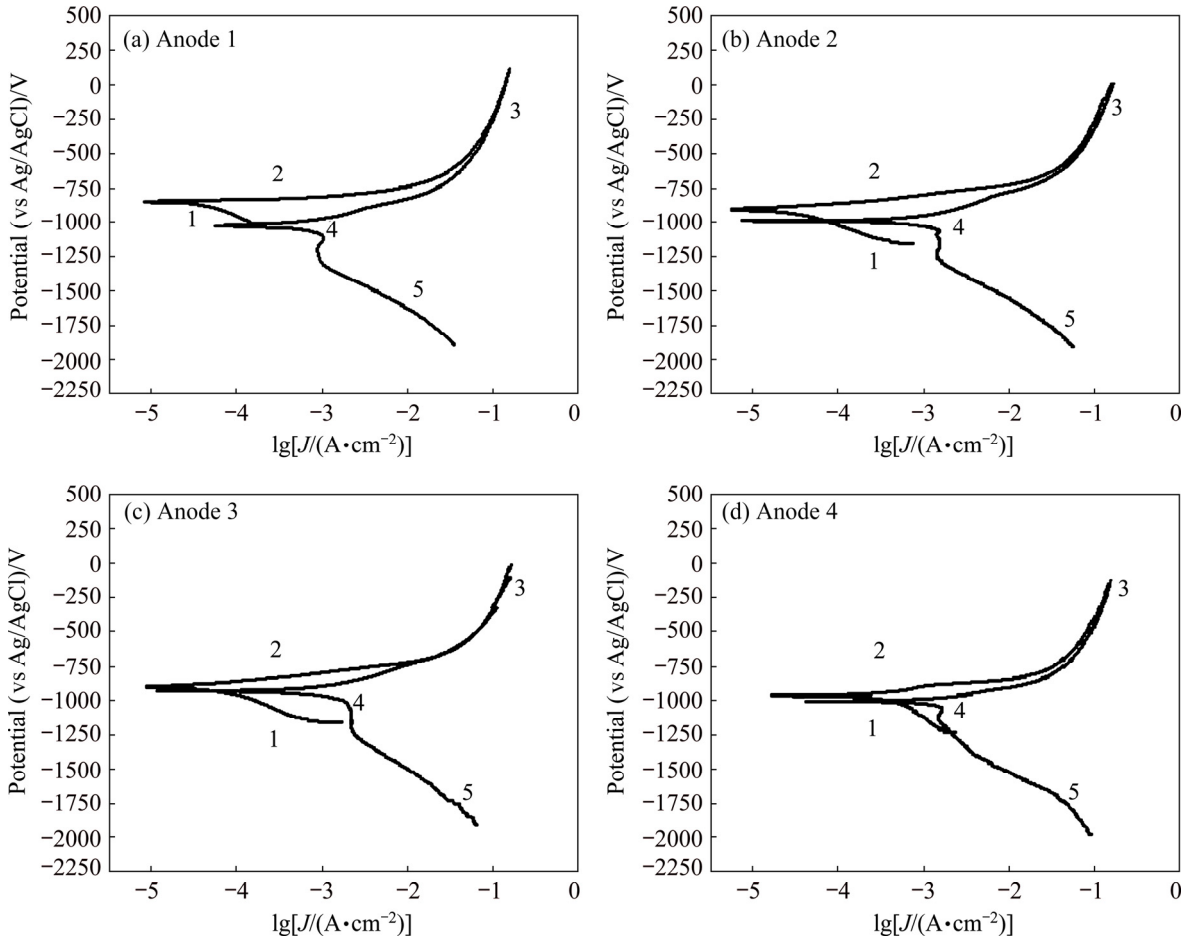

Fig. 8 Cyclic polarization of Al−Zn−Mg anodes with different Zn/Mg mass ratios in 3.5 wt.% NaCl solution

Table 5 Cyclic polarization parameters of Al−Zn−Mg with different Zn/Mg mass ratios in 3.5 wt.% NaCl solution

Anode No.	φ_{pit}/mV	J_{pit}/(A·cm^{-2})	φ_{pas}/mV	J_{pas}/(10^{-2}A·cm^{-2})	φ_{prot}/mV	J_{prot}/(10^{-4}A·cm^{-2})
1	130±6	0.311±0.01	−700±5	2.16±0.3	−1050±4	5.31±0.2
2	80±4	0.265±0.04	−675±3	4.16±0.4	−1055±3	7.61±0.1
3	−5.0±0.6	0.221±0.03	−660±4	7.16±0.1	−1010±5	9.21±0.2
4	−125±5	0.197±0.02	−645±6	8.16±0.2	−1060±2	9.51±0.3

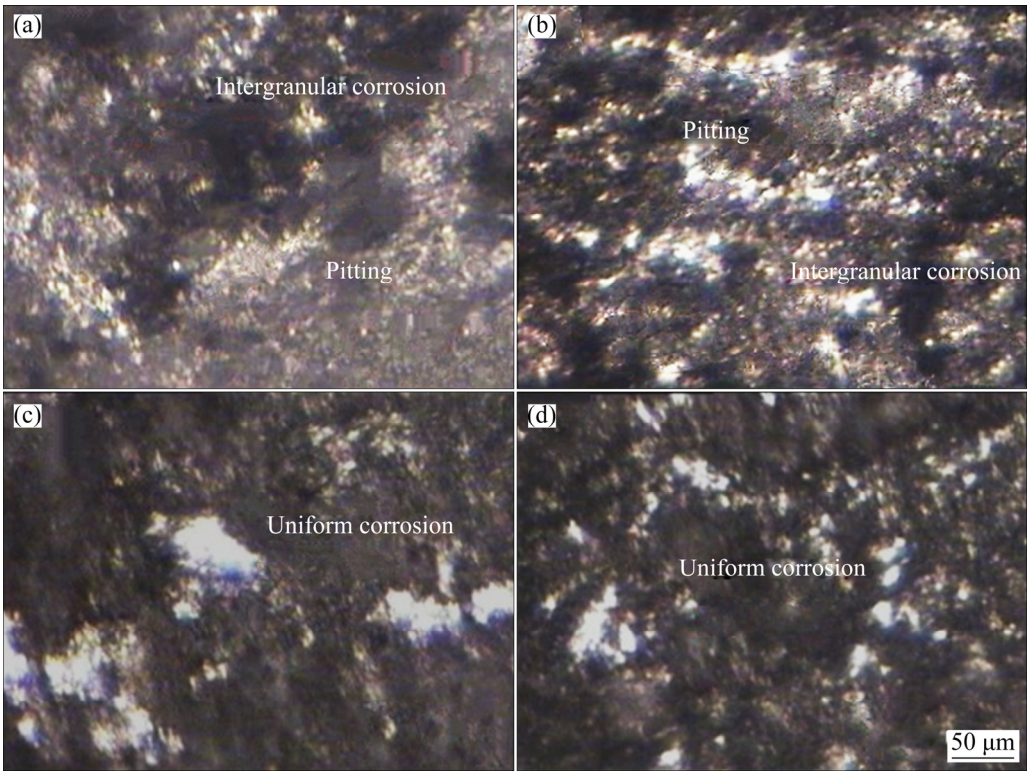

Fig. 9 Optical micrographs of surface morphologies of anodes after cyclic polarization tests: (a) Anode 1; (b) Anode 2; (c) Anode 3; (d) Anode 4

Optical morphologies of the investigated ingots after cyclic polarization are shown in Fig. 9. The morphologies illustrate that all ingots heavily corroded with black layers of corrosion products. However, ingots 1 and 2 display wide pitting with individual and cluster pits. The width of pits grows with increasing Zn/Mg mass ratio due to dissolution of the intermetallic precipitates which have larger sizes. Figure 9 also shows that Anodes 3 and 4 exhibit uniform corrosion with friable black layers.

3.3 Cathodic protection

Figure 10 shows the effect of Zn/Mg mass ratio on the open circuit potential (φ_{OCP}) of Al−Zn−Mg sacrificial anodes connected with steel for 90 d in 3.5 wt.% NaCl. It is obvious that the potentials of all the specimens move towards negative potential due to the dissolution of anodes. However, when the immersion time prolongs, Anodes 1 and 2 move towards the positive direction. The behavior is related to passivation of the surface and deposition of compact corrosion products making these anodes nobler compared to carbon steel. Also, Fig. 10 shows that Anodes 3 and 4 do not change significantly. This means that the corrosion products formed on their surfaces are friable. Consequently, the galvanic reactions on their surfaces are stable under this condition.

The SEM morphologies of Al−Zn−Mg ingots with different Zn/Mg mass ratios and steel after cathodic protection tests for 90 d in 3.5 wt.% NaCl are shown in Fig. 11. It is clear that all anodes heavily corroded with black thick corrosion products cover all surfaces, Further, the corrosion products on the surfaces of ingots 1 and 2 are compact and hard to be stripped from the α(Al)

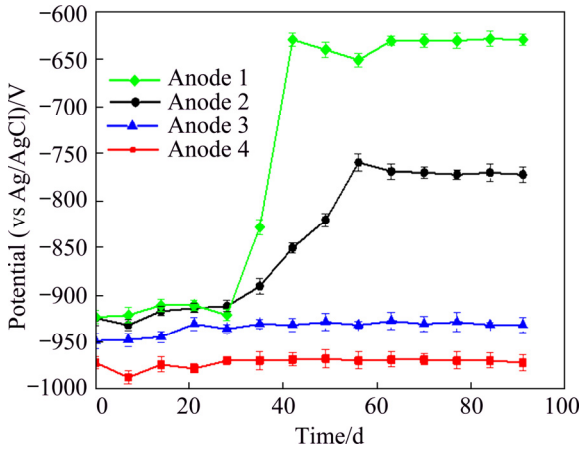

Fig. 10 Effect of Zn/Mg mass ratio on φ_{OCP} of Al−Zn−Mg sacrificial anodes connected with steel in 3.5 wt.% NaCl solution

matrix. The compact layers impede the electrochemical reaction of these ingots with NaCl and decrease the electrochemical activity. As discussed above, this behavior is owing to increasing the grain size of α(Al) and reducing volume fraction of the intermetallic precipitates, leading to providing more protective passive zones on the surface. Furthermore, ingots 1 and 2 suffer from localized corrosion when the aggressive ions attack their surfaces. It can be seen that the pitting corrosion locates at the center of the intermetallic precipitates and the size of pit increases with increasing Zn/Mg mass ratio. This is due to growing of pits and dissolution of precipitates around the grain boundaries.

Figure 12 displays the effect of Zn/Mg mass ratio on the corrosion rate of anodes connected to steel. It is obvious that Anodes 1 and 2 exhibit the lowest corrosion rate due to formation of compact passive film, while Anodes 3 and 4 exhibit the highest corrosion rate compared with the other anodes. This behavior is attributed to low compact corrosion products on their surfaces. The corresponding corrosion rates of steel connected to these anodes after 90 d of immersion in 3.5 wt.% NaCl are shown in Fig. 13. It can be seen that the corrosion rate of steel connected to Anode 1 is the highest due to passivation of this anode, while the corrosion rate of steel connected to Anode 4 is the lowest owing to continuous supplying of galvanic current obtained from this anode. The cathodic protection efficiency of steel with these anodes is shown in Fig. 14. It is obvious that the cathodic protection of steel increases with the decrease of Zn/Mg mass ratio. Further, Fig. 15 shows that the

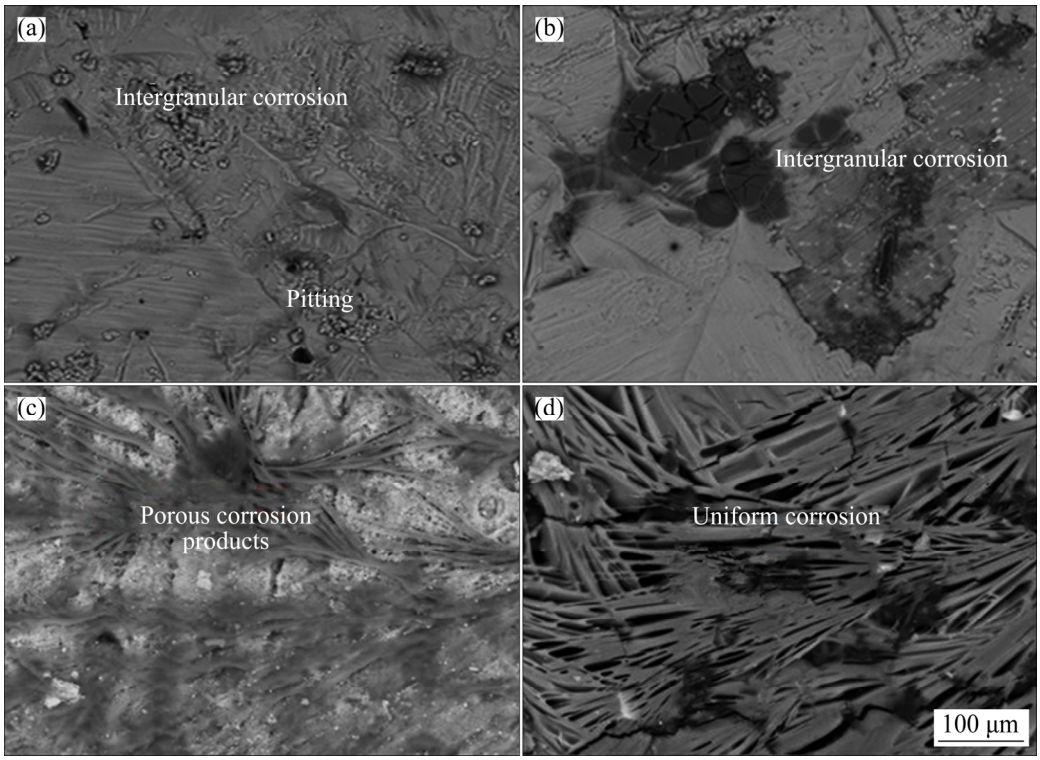

Fig. 11 Effect of Zn/Mg mass ratio on surface morphologies of Al−Zn−Mg sacrificial anodes connected with steel in 3.5 wt.% NaCl solution for 90 d: (a) Anode 1; (b) Anode 2; (c) Anode 3; (d) Anode 4

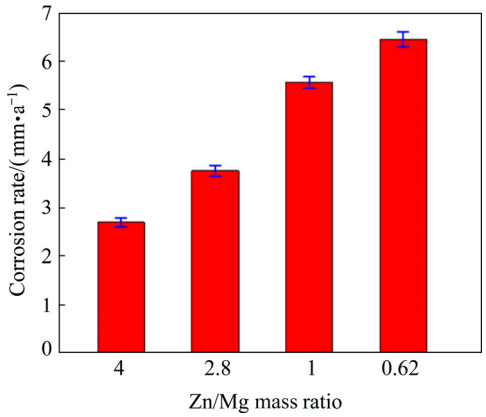

Fig. 12 Effect of Zn/Mg mass ratio on corrosion rate of Al−Zn−Mg sacrificial anodes connected with steel in 3.5 wt.% NaCl solution

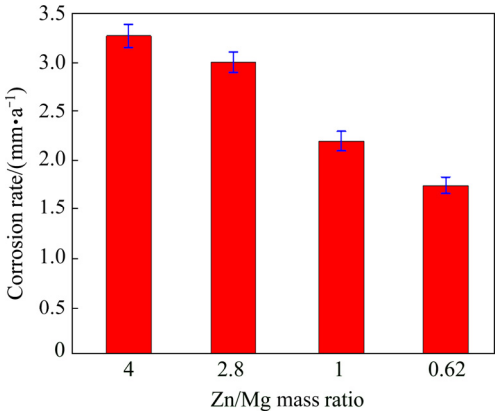

Fig. 13 Effect of Zn/Mg mass ratio on corrosion rate of steel connected with Al−Zn−Mg sacrificial anodes in 3.5 wt.% NaCl solution

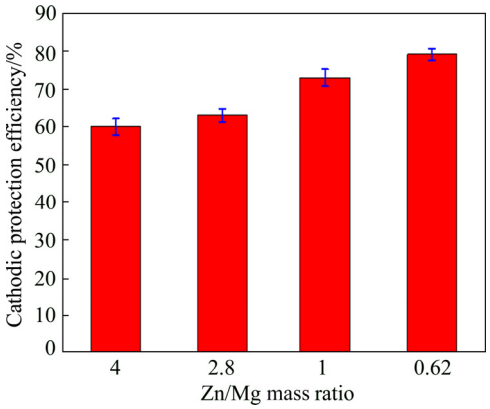

Fig. 14 Effect of Zn/Mg mass ratio on cathodic protection efficiency of steel connected with different Al−Zn−Mg sacrificial anodes in 3.5 wt.% NaCl solution

steel samples connected to the different anodes give different morphologies based on the Zn/Mg mass ratio of the anodes. The steel samples connected to Anodes 1 and 2 show heavy corrosion attack. This behavior is due to the passivation of these anodes which in turn impede the galvanic reaction and diminish the galvanic current required to cathodic protection. Figure 15 also reveals that steel samples connected to Anodes 3 and 4 exhibit low corrosion attack after 90 d in 3.5 wt.% NaCl. This means that these anodes provide galvanic current to protect the steel samples.

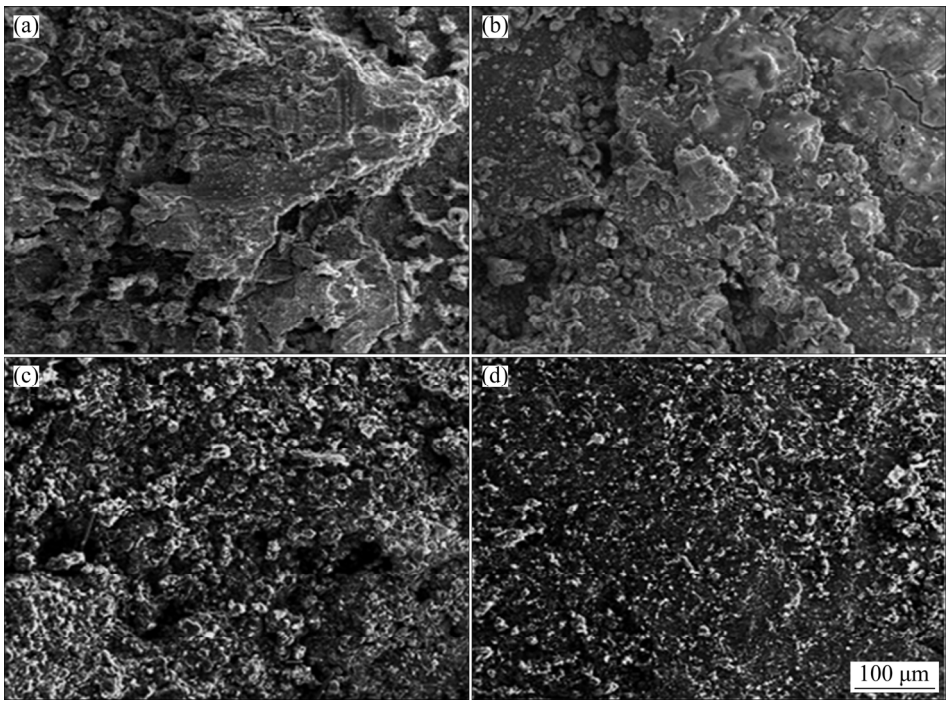

Fig. 15 Effect of Zn/Mg mass ratio on morphologies of steel connected with Al−Zn−Mg sacrificial anodes in 3.5 wt.% NaCl solution for 90 d: (a) Anode 1; (b) Anode 2; (c) Anode 3; (d) Anode 4

4 Conclusions

(1) The grain size of α(Al) and the particle size of the precipitates decrease while the volume faction of the precipitates increases with decreasing Zn/Mg ratio in Al−Zn−Mg sacrificial anodes.

(2) The anode with Zn/Mg mass ratio >4.0 exhibits the lowest corrosion rate, while the anode with Zn/Mg mass ratio <0.62 gives the highest corrosion rate and provides the highest cathodic protection efficiency for carbon steel. Furthermore, the results show that the anode with Zn/Mg mass ratio <0.62 exhibits a porous corrosion product comparing to the other anodes.

(3) The pitting corrosion locates at the center of the intermetallic precipitates and the size of pit increases with increasing Zn/Mg mass ratio.

References

[1] SHIBLI S M A, ARCHANA S R, ASHRAF P M. Development of nano cerium oxide incorporated aluminium alloy sacrificial anode for marine applications [J]. Corrosion Science, 2008, 50: 2232−2238.

[2] MA J, WEN J. The effects of lanthanum on microstructure and electrochemical properties of Al−Zn−In based sacrificial anode alloys [J]. Corrosion Science, 2009, 51: 2115−2119.

[3] FERDIAN D, PRATESA Y, TOGINA I, ADELIA I. Development of Al−Zn−Cu alloy for low voltage aluminum sacrificial anode [J]. Procedia Engineering, 2017, 184: 418−422.

[4] MA J, WEN J, ZHAI W, LI Q. In situ corrosion analysis of Al−Zn−In−Mg−Ti−Ce sacrificial anode alloy [J]. Materials Characterization, 2012, 65: 86−92.

[5] PINO M, CHACÓN J, FATÁS E, OCÓN P. Performance of commercial aluminium alloys as anodes in gelled electrolyte aluminium-air batteries [J]. Journal of Power Sources, 2015, 299: 195−201.

[6] GUDIĆ S, SMOLJKO I, KLIŠKIĆ M. Electrochemical behaviour of aluminium alloys containing indium and tin in NaCl solution [J]. Materials Chemistry and Physics, 2010, 121: 561−566.

[7] LI L, LIU H, YAN Y, ZHU H, FANG H, LUO X, DAI Y, YU K. Effects of alloying elements on the electrochemical behaviors of Al−Mg−Ga−In based anode alloys [J]. International Journal of Hydrogen Energy, 2019, 44: 12073−12084.

[8] LIU F, ZHANG J, SUN C, YU Z, HOU B. The corrosion of two aluminium sacrificial anode alloys in SRB-containing sea mud [J]. Corrosion Science, 2014, 83: 375−381.

[9] JINGLING M A, JIUBA W, GENGXIN L I, CHUNHUA X V. The corrosion behaviour of Al−Zn−In−Mg−Ti alloy in NaCl solution [J]. Corrosion Science, 2010, 52: 534−539.

[10] ABD EL ALL M I, SADAWY M M. Influence of ECAP as grain refinement technique on microstructure evolution, mechanical properties and corrosion behavior of pure aluminum [J]. Transactions of Nonferrous Metals Society of China, 2015, 25: 3865−3876.

[11] WAN H, HUANGFU W, LIU Z, DU C, LI X, SONG D, CAO B. Influence of sea mud state on the anodic behavior of Al−Zn−In−Mg−Ti sacrificial anode [J]. Ocean Engineering, 2017, 136: 11−17.

[12] SRINIVASA M, ADAPAKA S K, NEELAKANTAN L. Solubility effects of Sn and Ga on the microstructure and corrosion behavior of Al−Mg−Sn−Ga alloy anodes [J]. Journal of Alloys and Compounds, 2016, 683: 647−665.

[13] FENG Y, LI X, WANG W, PENG C, LIU L. Influence of cerium on microstructures and electrochemical properties of Al−Mg−Sn−Hg anode materials for seawater battery [J]. Journal of Rare Earths, 2015, 33(9): 1010−1015.

[14] FENG Y, LIU L, WANG R, PENG C, WANG N. Microstructures and electrochemical corrosion properties of Mg−Al−Pb and Mg−Al−Pb−Ce anode materials [J]. Transactions of Nonferrous Metals Society of China, 2016, 26: 1379−1387.

[15] TAN J, NISANCIOGLU K. Effect of small amounts of alloyed tin on the electrochemical behavior of aluminium in sodium chloride solution [J]. Corrosion Science, 2013, 76: 219−230.

[16] KARAMINEZHAAD M, JAFARI A H, SARRAFI A, SAFI G. Influence of bismuth on electrochemical behavior of sacrificial aluminum a node [J]. Anti-Corrosion Methods and Materials, 2006, 53(2): 102−109.

[17] BARBUCCI A, CABOT P L, BRUZZONE G, CERISOLA G. Role of intermetallics in the activation of Al−Mg−Zn alloys [J]. Journal of Alloys and Compounds, 1998, 268: 295−301.

[18] FAYED S M, SADAWY M M, MAHDY A A, ABDEL-KARIM R, ATLAM A. Evaluation of heat treated Al−Zn−Mg alloy as anode in KOH electrolyte for aluminium-air batteries [J]. Al-Azhar Bulletin of Science, 2016, 27: 1−12.

[19] SADAWY M, ZOHDY K. Effect of tin on the corrosion and electrochemical behavior of Al−Zn−Mg alloy in sea water [C]//Proc Light Metals 2014. PA: TMS, 2014: 383−388.

[20] OROZCO R, GENESCA J, JUAREZ-ISLAS J. Effect of Mg content on the performance of Al−Zn−Mg sacrificial anodes [J]. Journal of Materials Engineering and Performance, 2007, 16: 229−235.

[21] MA J, WEN J, LI Q, ZHANG Q. Effects of acidity and alkalinity on corrosion behaviour of Al−Zn−Mg based anode alloy[J]. Journal of Power Sources, 2013, 226: 156−161.

[22] YANG W, JI S, ZHANG Q, WANG M. Investigation of mechanical and corrosion properties of an Al−Zn−Mg−Cu alloy under various ageing conditions and interface analysis of η' precipitate [J]. Materials and Design, 2015, 85: 752−761.

[23] MANDAL P K, ANANT R, KUMAR R, MUTHAIAH V M R. Effect of scandium on ageing kinetics in cast Al−Zn−Mg alloys [J]. Materials Science & Engineering A, 2017, 696: 257−266.

[24] SUN H, LIU L, LI Y, MA L, YAN Y. The performance of Al−Zn−In−Mg−Ti sacrificial anode in simulated deep water

environment [J]. Corrosion Science, 2013, 77: 77−87.
[25] VALDEZ S, SUAREZ M, FREGOSO O A, JUÁREZ-ISLAS J A. Microhardness, microstructure and electrochemical efficiency of an Al (Zn/*x*Mg) alloy after thermal treatment [J]. Journal of Materials Science & Technology, 2012, 28(3): 255−260.
[26] QUEVEDO M C, GALICIA G, MAYEN-MONDRAGON R, LLONGUERAS J G. Role of turbulent flow seawater in the corrosion enhancement of an Al−Zn−Mg alloy: An electrochemical impedance spectroscopy (EIS) analysis of oxygen reduction reaction (ORR) [J]. Journal of Materials Research and Technology, 2018, 7(2): 149−157.
[27] ZHANG N, CHEN F, JIN Y, WANG J, JIN T, KOU B. Alloying effect in silver-based dilute nanoalloy catalysts for oxygen reduction reactions [J]. Journal of Catalysis, 2020, 384: 37−48.
[28] RALSTON K D, BIRBILIS N. Effect of grain size on corrosion: A review [J]. Corrosion, 2010, 66(7): 1−7.

锌镁比对 Al−Zn−Mg 牺牲阳极用于碳钢阴极保护的影响

Mosaad SADAWY[1], Saad SAAD[1], Randa ABDEL-KARIM[2]

1. Department of Mining and Petroleum Engineering, Faculty of Engineering, Nasr City, Al-Azhar University, Cairo 11371, Egypt;
2. Department of Metallurgy, Faculty of Engineering, Cairo University, Giza 12613, Egypt

摘　要：研究不同锌镁质量比的 Al−Zn−Mg 合金作为牺牲阳极在 3.5wt.%NaCl 溶液中用于碳钢阴极保护的性能。用纯 Al、Zn 和 Mg 金属通过铸造法制备 Al−Zn−Mg 阳极。采用光学显微镜、扫描电镜−能谱、X 射线衍射和电化学等技术对样品进行表征和测试。结果表明，随着锌镁质量比的降低，α(Al)的晶粒尺寸和析出物的粒径减小，析出物的体积分数增大。当锌镁质量比大于 4.0 时，Al−Zn−Mg 阳极具有最低的腐蚀速率；当锌镁质量比小于 0.62 时， Al−Zn−Mg 阳极具有最高的腐蚀速率且对碳钢(AISI 1018)具有最好的阴极保护效果。与其他阳极相比，锌镁质量比为 0.62 的 Al−Zn−Mg 阳极具有多孔腐蚀产物。

关键词：阴极保护；Al−Zn−Mg 牺牲阳极；电流容量；钝化膜；析出物；晶粒尺寸

(Edited by Xiang-qun LI)